Electron-spectroscopic manifestations of the 4f states in light rare-earth solids

W.-D. Schneider, B. Delley, E. Wuilloud, J.-M. Imer, and Y. Baer

Institut de Physique, Université de Neuchâtel, CH-2000 Neuchâtel, Switzerland

(Received 26 June 1985)

The consequences of the degeneracy between configurations with different populations of atomic-like f states are studied systematically for a number of light rare-earth materials (Ba, LaF_3, La_2O_3, La, CeO_2, $CeCo_2$, CeN, α-Ce, and γ-Ce) using high-energy spectroscopies. The Anderson impurity model applied to this problem (Gunnarsson-Schönhammer model) is found to describe convincingly a variety of electron-spectroscopic excitations, such as, x-ray photoemission and bremsstrahlung isochromat spectroscopy. We have extended this many-body formalism to account for electron-energy loss spectroscopy and L_{III} absorption edges. The parameters resulting from the calculation are analyzed within the framework of a simplified Hamiltonian containing no coupling terms between f and band states. This approach reveals in a natural way the importance of the conventional concept of hybridization. The energy degeneracy and the wave-function overlap of quantum states give rise to a mixing and to a continuous energy distribution of excitations. For electronic transitions described within the sudden approximation the impurity model provides a sound and unified description of the "satellite complex" encountered in the high-energy excitation spectra of such systems.

I. INTRODUCTION

Since the early days of photoelectron spectroscopy, the appearance of satellite lines in core-level spectra has been the subject of many investigations.[1-17] It was recognized that these satellites are closely related to the presence of open $3d$, $4f$, and $5f$ shells. Numerous interpretations were given to correlate their intensity and energy positions with the ground-state properties of the solid. For example, in actinide compounds, the appearance of satellite lines in core-level spectra was considered as precursory indication of f-electron localization.[12,13] In the rare-earth compounds, the occurrence of two sets of structures in core-level spectra has been interpreted quite often in terms of two localized $4f$ populations.[14] However, in the earliest x-ray photoemission studies of atoms and molecules[1] it was recognized that the sudden potential change resulting from the ionization of a deep core level can induce drastic modifications among the outer electrons: Simultaneous excitations within the outer bound levels can occur or additional weakly bound electrons can be expelled. These two types of processes were called, respectively, electron "shakeup" and electron "shakeoff." Since the main weight of the spectra is usually concentrated on the simple ionization process, the weak structures at larger binding energies corresponding to these additional excitations were considered as satellites. Within the Hartree-Fock approximation and the sudden approximation the necessity of such excitations and the relationship between their distribution and the relaxation energy is rather straightforward.[18] The multiplet splitting resulting from the exchange and electrostatic interactions of incomplete shells will be discarded here. In solids, strong core-level satellites have been first observed in core-level excitations of ionic compounds.[2,3] In an atomiclike model, their origin

can be relatively simply explained by a configuration-interaction between distinct final states being close in total energies. At about the same time, a splitting into two components of comparable intensities has been observed in $3d_{3/2,5/2}$ core-level spectra of light rare-earth ionic compounds such as, for example, La_2O_3.[4,5] In the original interpretation, the high-binding-energy peaks were considered as an energy-loss or shakeup process described as a charge transfer from filled ligand orbitals to the empty $4f$ shell after creation of the core hole. A few years later, the observation of three peaks in the core-level spectra of CeO_2 led Burroughs et al.[19] to the idea that the presence of a core hole can lower substantially the $4f$ energy relative to the band states, so that the population of a $4f$ state can be the most efficient screening mechanism. For this type of screening transition the terms "energy gain" or "shakedown" satellites have been coined. This picture has been extended by Crecelius et al.[20] to the weak $3d$ low-binding-energy satellites observed in the light rare-earth metals.

The first attempts to go beyond an atomiclike description of such satellites in solids have been made by Kotani and Toyozawa[15,16] and Schönhammer and Gunnarsson.[17] They provided a quantitative description in terms of core-hole screening populations originating from coupled states with different symmetries and spatial extents. These approaches represent an important first step toward the more elaborate calculations available today. They are at the origin of the nowadays popular but too schematic expressions "well-screened" and "poorly-screened" final states used for characterizing respectively a low- and a high-binding-energy core line in rare-earth, actinide, and transition elements.[21] At the present time, the accumulation of spectra containing core-level and valence-band satellites demonstrates that this type of manifestation ac-

counts for a rather general situation which is certainly unconventional but not exceptional. Presently the Anderson impurity model appears to provide the simplest framework for describing the excitations of rather localized states which are hybridized with band states. After the first approach of Oh and Doniach,[22] a unified and quantitative many-body calculation scheme for the various core-level and outer-level excitations in Ce has been proposed by Gunnarsson and Schönhammer.[23] Ce with its low $4f$ population offers the simplest conditions for studying this mixing mechanism which has a dominating influence on the spectra and is not involved with complex multiplet structures. The achievements of this model are the following.

(i) A single set of parameters, characterizing the electronic structure of a solid, yields correctly all kinds of excitation spectra. This allows one to reconcile the contradictory pictures of the $4f$ states deduced from the different experimental techniques [x-ray photoemission (XPS), bremsstrahlung isochromat spectroscopy (BIS), electron-energy loss spectroscopy (EELS), x-ray absorption spectroscopy (XAS), susceptibilities, and lattice constants[24–28]].

(ii) The correct width of the bands included into the model allows one to predict the spread and shape of the $4f$ and core spectra in a more realistic way than in any cluster calculation.[29]

(iii) Mixing in initial and final states are taken into account. In both states the $4f$ population is found to be integral only in extreme situations. This invalidates the atomic description and calls in question the use of deep core-level spectroscopy for revealing valence fluctuations.

The aim of this paper is to present and to analyze the electron spectroscopic manifestations of the $4f$ states in a particular sequence of solids where the consequences of f admixture to the band states can be studied in a systematic manner. Despite the hidden aspects of the theoretical computation the behavior of the spectra allows one to understand intuitively how the parameters used to characterize the electronic structure determine the observed excitations.

II. EXPERIMENTAL DETAILS

With the exception of the spectra of La_2O_3 and $CeCo_2$, the data shown and discussed in this work have been taken from already published studies, those of Ba (Refs. 30—33) and LaF_3 (Refs. 7, 34, and 35) as well as of the valence bands of γ-Ce and α-Ce (Ref. 36) have been measured by other authors, those of La (Refs. 37 and 38), CeO_2 (Ref. 39), CeN (Refs. 40—41), α-Ce, and γ-Ce (Ref. 27) originate from the present authors. All our spectra have been obtained in a single instrument which allows us to perform XPS, BIS, and EELS on the same sample without breaking the vacuum of 2×10^{-11} Torr.[42,37]

The La_2O_3 sample was prepared in situ from La films freshly evaporated on Cu and oxidized at 300 K in an oxygen atmosphere of 10^{-6} Torr for 6 h. Subsequently the films were exposed for 10 min to an oxygen discharge at 0.1 Torr in order to obtain sufficiently thick La_2O_3 samples. By varying the photon flux or the electron beam current during the different measurements, no charging effect could be detected. The relative position of the energy scales in the XPS and BIS spectra of La_2O_3 were calibrated within 0.1 eV by observing with both techniques the position of the Fermi level (E_F) of a Ag film deposited onto La_2O_3.

The polycrystalline $CeCo_2$ sample was prepared by melting the constituents in a levitation furnace. An x-ray analysis confirmed the Laves phase structure of the compound and no foreign lines due to other phases were detected. Clean surfaces were obtained in situ by scraping with an Al_2O_3 file. In order to avoid a rapid surface accumulation of oxygen diffusing from the bulk, the sample was held at liquid-nitrogen temperature.

III. THE MODEL

We have analyzed the XPS, BIS, and EELS spectra within the Gunnarsson-Schönhammer (GS) approach[23] which was originally developed for describing different spectroscopic transitions in metallic Ce compounds. We have adapted this model for L_{III} absorption edges[43] and EELS transitions and we have extended it to insulating rare-earth compounds. In this section we give only a discussion of the model relevant to XPS and BIS. The EELS and L_{III} edges will be treated separately in Secs. VI and VII, respectively. The electronic density of states of insulators was simulated by semielliptical valence and conduction bands separated by a gap. We note, that the large f degeneracy N_f is much less important for insulators than for metals since no low-lying bandlike excitations could lead to divergencies. The calculations have been performed to second order in $1/N_f$ (Ref. 23) and they include basis states up to double f occupation. Lower-order approximations which are useful for Ba metal and La compounds are discussed in the Appendix.

For each compound, the heights, widths, and positions of the bands have been chosen in such a way that the model can account correctly for the mixing of the $4f$ states with the extended states. This schematic band picture represents a weighted density of states (DOS) where the amplitude is proportional to the coupling strength Δ defined in the Appendix. The relevant DOS features are respected, but need not be more realistic since the aim of the model calculation is exclusively the description of the $4f$ contributions to the different excitations. The computed spectra have been compared to all experimental spectra (XPS, BIS, EELS) and the parameters have been varied until the best general agreement is found. In fact, this procedure represents a stringent test of the model. In this way, more reliable parameter values are obtained than by a fit to only one type of experimental spectrum. Among the parameters, the f-f Coulomb repulsion U_{ff} and the Coulomb attraction U_{fc} of the $4f$ states by a core hole are essentially atomic quantities which are renormalized by the screening mechanisms in solids. As shown in Table I, their values do not scatter very much among the different

TABLE I. Relevant energies (eV) and populations obtained from the fit of the many-body calculations to the experimental spectra.

Material	Δ_{fp}	Δ_{fd}	ϵ_f	U_{ff}	U_{fc}	n_f
Ba		0.1	14.0	8	-12	0.003
LaF$_3$	0.6	0.06	14.5	8	-13.5	0.002
La$_2$O$_3$	0.6	0.06	10.7	8	-12	0.04
La		0.08	5.5	8	-9	0.01
CeO$_2$	0.6	0.06	0.5	8	-12	0.45
CeCo$_2$		0.3	-1.2	5.5	-10	0.76
CeN	0.2	0.1	-0.8	7	-11	0.80
α-Ce		0.08	-1.2	6	-10	0.88
γ-Ce		0.03	-1.5	6	-10	0.98

types of solids considered. Only two parameters remain completely free in the fitting procedure: the hybridization energy Δ defined in the Appendix, and ϵ_f representing in the limit of $\Delta = 0$ and $U_{ff} = 0$, the energy difference between consecutive f counts. The values of the initial $4f$ populations n_f, also given in Table I have not been adjusted but they are a result of the model calculation.

Once all these parameters are known from the model calculation, it is very instructive to take a step backwards and to discuss the results within the framework of a simplified Anderson impurity Hamiltonian without the hopping term:

$$H_u = \sum_k \epsilon_k n_k + \epsilon_f \sum_m n_m + U_{ff} \sum_{m' > m} n_{m'} n_m$$
$$+ n_c \epsilon_c + (1 - n_c) U_{fc} \sum_m n_m .$$

The orbital indices m and k for the $4f$ and valence states implicitly include the spin. We note that the parameters entering the uncoupled Hamiltonian H_u can be estimated in principle from a parameter free density-functional calculation.[44] For the discussion of excitation spectra it is convenient to choose as an origin of the total-energy scale the total electronic energy of the ground-state configuration (this definition remains valid for the model calculation). In this simple scheme the population changes induced in the bands, $4f$ levels or core levels, are assumed to be screened by charge transfer among the highest occupied band states. This mechanism corresponds to a negligible variation of the Fermi-energy position in a metal and it supposes the creation of a polarization charge originating from the valence-band top in an insulator. This assumption appears to provide the correct way to relate on a total-energy scale the single-particle excitations of extended states to the total energies involved in population variations of highly correlated states. Within this simple framework ($\Delta = 0$), the density of the single-particle excitations of the outer levels, relevant for these spectroscopies, will be called "uncoupled $S(E_t)$." This quantity is composed of the weighted density of states discussed previously and of the discrete spectrum for uncoupled f states. As shown in Fig. 1 this uncoupled $S(E_t)$ can be split into electron-addition and electron-subtraction processes which must be represented on a common total-energy scale in order to be consistent with the Hamiltonian. It is more usual to represent these two types of excita-

tions within a single-particle excitation spectrum where the states are given as a function of the energy of one electron occupying the considered level. This representation is just obtained from the previous one by a 180° rotation
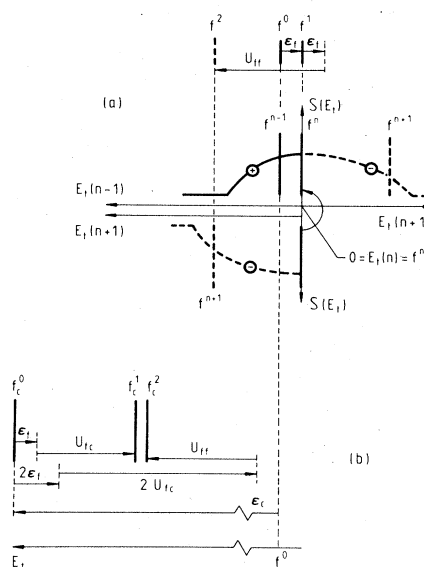

FIG. 1. (a) Screened single-particle excitations of the extended and localized outer levels without coupling as a function of the total electronic energy E_t of the final state: uncoupled $S(E_t)$. Left part: uncoupled $S(E_t)$ resulting from the addition (thick dashed lines) and subtraction (solid lines) of one electron represented separately on a common total-energy scale. The position of f^n represents the total energy of the ground state and does not belong to the excitation spectrum. The parameters linking the different $4f$ populations shown in the top of the figure are correct only for an uncoupled $4f^1$ ground state. Right part: the uncoupled $S(E_t)$ for electron addition rotated by 180° around the origin in order to make it consistent with the usual single-particle representation of the excitation spectra (XPS + BIS). (b) Lowest total energies of the different uncoupled final states in the presence of a core hole for an f^1 ground state. This diagram is most conveniently constructed by starting from the total energy of an initial $4f^0$ configuration. The creation of a core hole raises this energy by ϵ_c. In addition to the other parameters one has now to take into account the core-hole attraction U_{fc}. The relative positions of the different final-state populations can be easily calculated from the simplified Hamiltonian.

of the electron-addition spectrum. For two atoms in an uncoupled ($\Delta = 0$) $4f^n$ ground-state configuration one can verify in the single-particle or total-energy representation that U_{ff} corresponds to the common definition of the Coulomb correlation energy involved in the formation of the two noninteracting polar states $4f^{n-1}$ and $4f^{n+1}$. When only f states are considered, one has to realize that their energy is given by

$$E_n(f^n) = n\epsilon_f + \tfrac{1}{2}n(n-1)U_{ff} .$$

This is just the parabolic behavior of the total energy as a function of the f population.

When the hopping terms accounting for the overlap in space of the $4f$ and band states are included, a hybridization can take place between these two kinds of states when they are not too far from the degeneracy. This mechanism becomes particularly important when the total energy of a neighbor configuration (f^{n+1} or f^{n-1}) approaches the total energy of f^n; ground states are formed with fractional f counts which can be very different from integral numbers. The virtue of the GS model is to provide a scheme for the calculation of these states and for the different excitation spectra within the sudden approximation. The complication of this hybridization problem originates from the energy spread of the band states and from the f degeneracy.

For the description of core-hole excitations it is convenient (but not absolutely necessary) to start from the total energy of the initial configuration f^0 even if it is not the ground-state configuration. In the presence of a core hole ($n_c = 0$), this energy is simply raised by ϵ_c as shown in Fig. 1(b). In the uncoupled scheme, it is then a simple matter to calculate the relative positions of the other final-state f populations by inserting the suitable numbers (Table I) in the simplified Hamiltonian. The simultaneous excitations of band states created in the core-hole ionization should be represented in Fig. 1(b) as continua extending from each f^n level toward higher total energies. For this reason the measured and computed excitation spectra show in some cases more complicated or extended structures than expected from the mixing of the narrow uncoupled states. As long as the different accessible f^n final states are well separated and/or the hybridization parameter Δ remains negligible, the position of the peaks in the core-level spectra are well predicted by the uncoupled energies. The intensity of each peak accounting for a practically integral f population reflects the strength of these configurations in the initial states.

An important final-state mixing can only occur when, simultaneously, the value of Δ is sizable and two uncoupled configurations with different f counts have nearly or completely degenerate total energies. Furthermore, the coupling is strong only if their f-population difference is one electron. In this case, split levels are formed by hybridization, each of them containing comparable contributions from the two uncoupled states. The weight of the two configurations forming the mixed states is no longer representative of the initial ground state. In such extreme situations, it makes no sense to attempt any identification of the two observed peaks in terms of different integral $4f$ populations and to interpret their ratio as the mixing of

the initial state. A discussion about the energy separation between these hybridized peaks is given in the Appendix. Finally, one should notice that the multiplet splitting has not been included in these calculations.

IV. SYSTEMS WITH $4f^0$ GROUND-STATE CONFIGURATION IN THE UNCOUPLED SCHEME

The systems selected and discussed in this section have in common the fact that in the uncoupled scheme ($\Delta = 0$) the total energy is larger in the $4f^1$ configuration than in the $4f^0$ configuration ($\epsilon_f > 0$). This means that without hybridization they would all be in a pure $4f^0$ ground state. In Fig. 2 these systems have been disposed vertically in a sequence where the energy difference ϵ_f decreases gradually. We shall consider at first the outer-level excitation spectra which are shown in Fig. 2(a) together with the corresponding uncoupled $S(E_t)$ and the model calculations. Except for CeO_2, discussed separately later, the influence of the hybridization remains negligible in the direct population changes induced in XPS and BIS. This is an obvious consequence of the large energy separating the $4f^0$ and $4f^1$ configurations. Even in LaF_3 and La_2O_3, where large values of Δ are obtained, the initial $4f^1$ population n_f is well below 0.1 and in the model calculation of the photoemission spectra its contribution can be barely discerned. Therefore, the structures observed in the XPS spectra must be interpreted as band excitations. The $4f$ contributions to the BIS spectra have been shaded in order to distinguish them from the population of extended states. Besides strong variations of the width, attributable to the lifetime broadening and to the different instrumental resolutions, the model calculation traces the f contributions of the BIS spectra very well. In these systems, with the exception of CeO_2, the model calculation for the outer-level excitations is not necessary, since it reproduces faithfully the energy positions of the uncoupled $4f^1$ states.

The situation becomes more interesting in CeO_2, where the uncoupled f^0 and f^1 energies are very close. This proximity and the large value of Δ give rise to a sizable mixing of f^1 with f^0 states responsible for the important initial $4f$ population $n_f \sim 0.5$. The fact that CeO_2 is an insulator constrains this ground-state mixing to occur within the full valence band, which must accommodate this f admixture of extended nature. This contribution does not exhaust all the available $4f^1$ states so that another type of $4f^1$ states is found at higher single-particle energies, in the range where the population of extended states is forbidden (band gap of the extended states). For this reason the admixture remains small in the gap where nearly pure $4f^1$ states are formed. The agreement of this description resulting from the impurity calculation with a band calculation is gratifying.[45] The weak $4f^1$ admixture to the valence band cannot be distinguished in the total XPS spectrum. The BIS spectrum is dominated by the $4f^1$ peak, whereas the broad $4f^2$ final states mixed with conduction-band states, are embedded into the signal originating from extended states and the background. There have been controversies in the literature whether compounds like CeO_2 should be called mixed valent or not.[46,47,29] According to Varma,[48] the term mixed valent
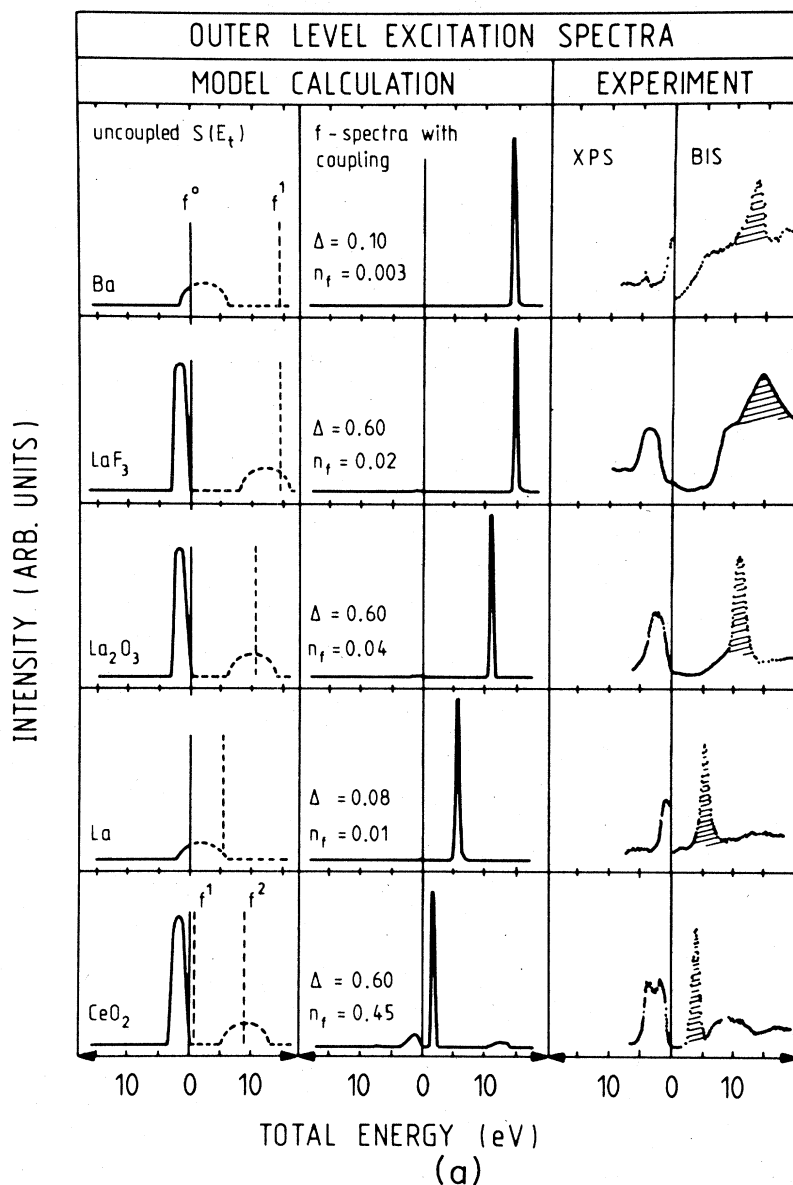
FIG. 2. (a) Calculated and measured outer-level excitation spectra. In the uncoupled $S(E_t)$ (see Sec. III), the amplitude of the valence and conduction bands is chosen proportional to the hybridization parameter Δ. In the calculation of the f spectra with coupling, a Gaussian instrumental broadening of 0.4 eV full width at half maximum (FWHM) has been included. The experimental spectra have been taken from the following works. XPS: Ba (Ref. 30); LaF$_3$ (Ref. 34); La$_2$O$_3$, La (this work); CeO$_2$ (Ref. 39). BIS: Ba (Ref. 32); LaF$_3$ (Ref. 35); La$_2$O$_3$, La (this work); CeO$_2$ (Ref. 39). The origin of the total-energy scale is the Fermi energy in metals and the upper valence-band edge in insulators. The f contribution corresponds to the hatched areas. (b) Calculated and measured $3d$ core-excitation spectra (see Sec. III). In the spectra with coupling the solid curves correspond to XPS and the dotted curve to EELS. The calculated spectra have been convoluted by a Lorentzian of 1.2 eV FWHM to include lifetime broadening. The experimental spectra have been taken from the following works. XPS: Ba (Ref. 30); LaF$_3$ (Ref. 7); La$_2$O$_3$, La (this work); CeO$_2$ (Ref. 39). EELS: Ba (Ref. 33); CeO$_2$ (Ref. 39). The XPS and EELS spectra have a common energy scale and the centers of gravity of the EELS final states are indicated by arrows in the corresponding XPS and EELS spectra.

characterizes the fractional occupation of localized states in metals. This is obviously not the case in CeO$_2$ where the Ce atoms are tetravalent, since no atomiclike localized f level is occupied and the four outer electrons are involved in the covalent p-d and p-f admixture to the chemical bond.

The XPS $3d$ core-level excitations displayed in Fig. 2(b)

contain many unconventional aspects, which can be easily understood by considering the initial-state situation described previously and the uncoupled final-state positions obtained [Fig. 1(b)] with the parameters given in Table I. (The discussion of EELS spectra is delayed to Sec. VI.) From Ba to La, the initial-state mixing is negligible and the ground-state configuration is nearly pure

3d CORE LEVEL EXCITATION SPECTRA

MODEL CALCULATION		EXPERIMENT	
uncoupled final state positions	spectra with coupling	XPS	EELS

Figure content (INTENSITY (ARB. UNITS) vs TOTAL RELATIVE ENERGY (eV)):

Ba — f_c^2 f_c^1 f_c^0 — $\Delta = 0.1$, $n_f = 0.003$ (XPS, EELS)

LaF$_3$ — f_c^2 f_c^1 f_c^0 — $\Delta = 0.6$, $n_f = 0.02$

La$_2$O$_3$ — f_c^2 f_c^0 f_c^1 — $\Delta = 0.6$, $n_f = 0.04$

La — f_c^2 f_c^0 f_c^1 — $\Delta = 0.08$, $n_f = 0.01$

CeO$_2$ — f_c^0 f_c^1 f_c^2 — $\Delta = 0.6$, $n_f = 0.45$; $\vdash^{3}/2\dashv \vdash^{5}/2\dashv$

Axes: $+10\ \varepsilon_c\ -10$ $+10\ \varepsilon_c\ -10$ 30 20 10 0   30 20 10 0

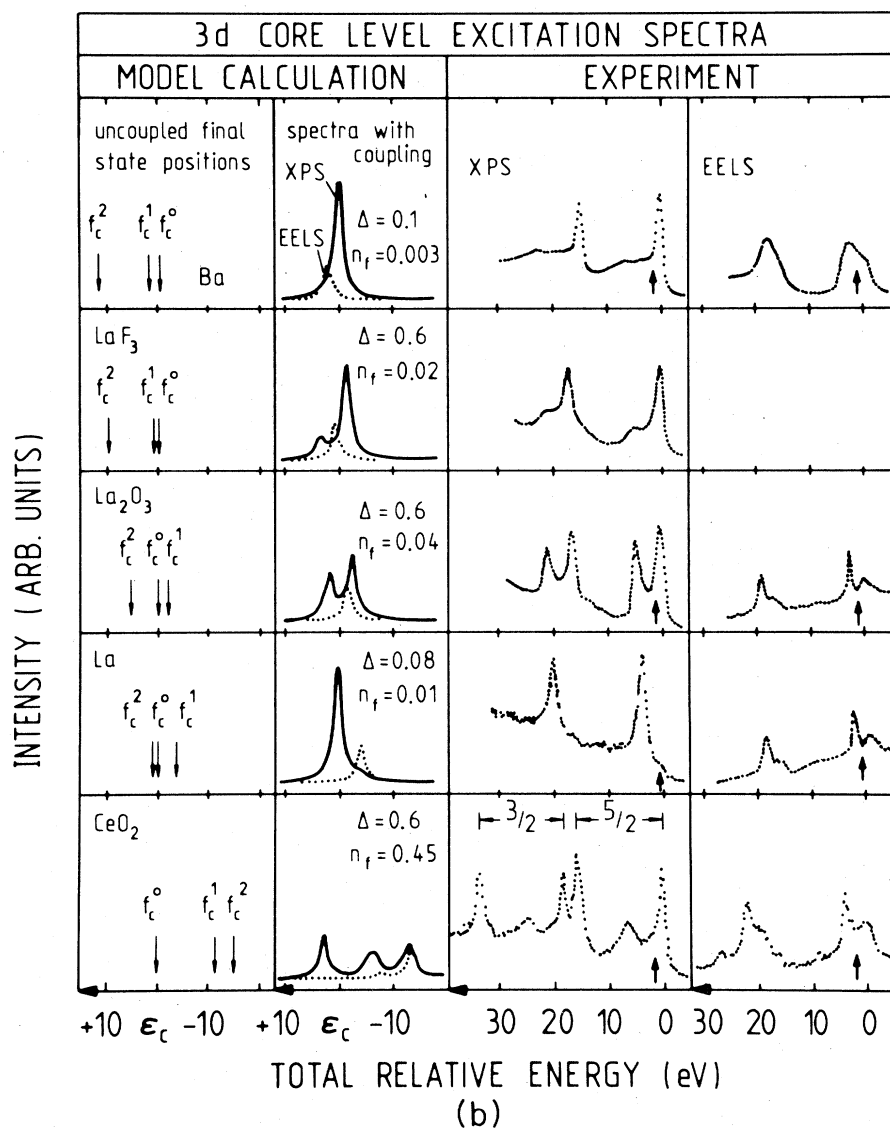TOTAL RELATIVE ENERGY (eV)

(b)

FIG. 2. (Continued).

$4f^0$. The presence of a core hole decreases dramatically the total-energy difference between the $4f^1$ and $4f^0$ configurations so that a final-state mixing becomes possible. In Ba metal the value of Δ is still too small to induce a detectable hybridization and the model predicts a simple Lorentzian line shape. The XPS $3d$ lines confirm this expectation since the pronounced asymmetry is due to electron-hole pair excitations not included in the model and the small satellite can be identified with a plasmon excitation.[49] In the insulator LaF$_3$, the value of the hybridization parameter Δ is now 0.6 eV and the resulting final-state mixing is responsible for the two peaks predicted and observed in the $3d$ core-level spectrum. In this case an identification of the two structures with different integral $4f$ populations is dubious and only the more intense one has a clearly dominant $4f^0$ component. In La$_2$O$_3$, the order of the f_c^1 and f_c^0 final-state positions is inverted and

the value of Δ is large again. The consequence is a splitting of the core-hole final state into two components of nearly equal intensities.[4,6,7,19,21,11] Each of them is formed by a mixing of the two configurations f_c^0 and f_c^1 in a ratio of approximately one to one and their separation is mainly determined by Δ (see Appendix). Furthermore, the analysis of the model calculation shows that in fact the excitation spectrum does not consist simply of two neighbor peaks, but corresponds to a continuous intensity distribution reflecting excitations of valence states through the whole bandwidth. La$_2$O$_3$ provides one typical example that demonstrates that the traditional interpretation of each peak in terms of pure atomic configurations is completely in error.

At this point it is interesting to consider briefly the evolution of the different excitation spectra of the trivalent-La compounds with F, O, Cl, and Br.[6,7] The decrease of
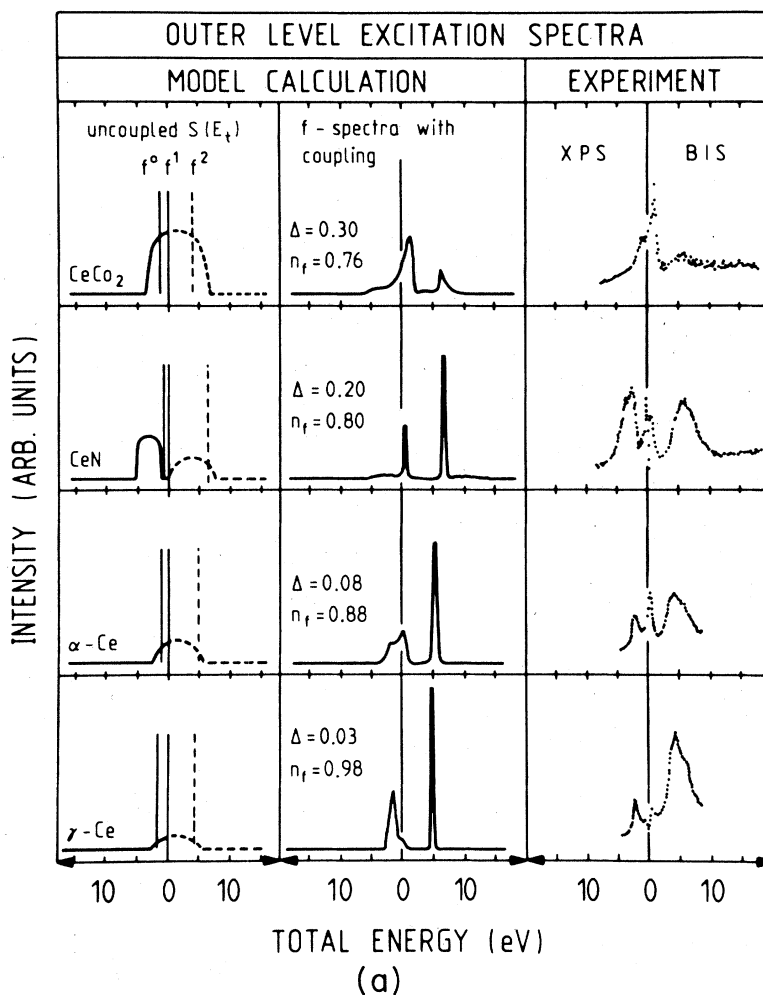
FIG. 3. (a) Calculated and measured outer-level excitation spectra [see caption of Fig. 2(a)]. The experimental results originate from XPS: $CeCo_2$ (this work), CeN (Ref. 41), α- and γ-Ce (Ref. 36); BIS: $CeCo_2$ (this work), CeN (Ref. 41), α- and γ-Ce (Ref. 27). (b) Calculated and measured $3d$ core-excitation spectra [see caption of Fig. 2(b)]. The experimental results originate from XPS: $CeCo_2$ (this work), CeN (Ref. 40), α- and γ-Ce (Ref. 27). EELS: $CeCo_2$ (this work), CeN (Ref. 41), α- and γ-Ce (Ref. 27).

electronegativity in this sequence[50] corresponds to an increase of the charge available for the screening around the La atom. This strengthening of the screening power with decreasing ligand electronegativity contributes certainly to the reduction of the total energy involved in the creation of core holes (chemical shifts). The same mechanism is assumed to be responsible for the important decrease of the $4f^1$ total energies observed in the BIS spectra of Fig. 2(a) for the sequence LaF_3, La_2O_3, La metal. Such shifts in inverse photoemission of localized levels are at variance with the conventional interpretation of the chemical shift based only on simple electrostatic considerations in the initial state. Proceeding now from La_2O_3 to $LaCl_3$ and $LaBr_3$, one can anticipate that the energy difference between f_c^0 and f_c^1 is still increasing. Assuming a constant Δ, the model calculation for this evolution of the uncoupled final-state energies shows that the intensity is transferred from the low-energy peak LaF_3 to the high-energy peak $LaBr_3$, in perfect agreement with the mea-

surements.[6,7] It is important to notice that in both extreme situations where the mixing is not too strong, the most intense peak has a dominant f^0 character reflecting the initial-state configuration. The model calculation appears to provide a sound and unified description of the La "satellites" which have given rise to so many intuitive interpretations.[4,6,11,19,21]

In La metal, f_c^0 and f_c^1 energies are not quite as close and Δ is small. Since the initial $4f^1$ population is negligible ($n_f = 0.01$) and the conditions for a final-state mixing are not favorable, the excitation spectrum contains essentially a leading f_c^0 peak accompanied by a weak f_c^1 satellite. In this case, nearly pure final-state configurations are realized. It is interesting to notice that from the f^0 initial state, the matrix element expressing the sudden approximation for a core-electron photoemission provides practically no intensity to the f_c^2 final state. Despite the fact that the two configurations f_c^2 and f_c^0 are nearly degenerate, the effective hybridization between states with f-
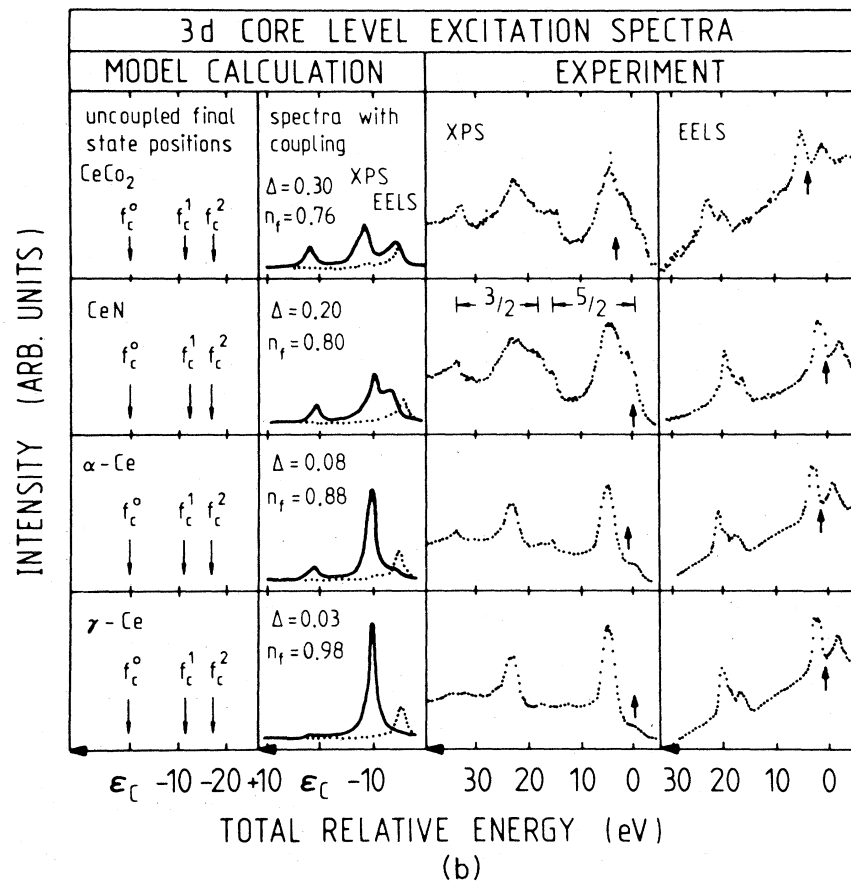
FIG. 3. (*Continued*).

count differences larger than one is negligible.

Finally, in CeO$_2$ the relative positions of the uncoupled energies of the different f^n configurations are drastically modified when a core hole is created. f_c^0 has now the highest energy and is well separated from f_c^1 and f_c^2. For this reason it cannot hybridize and consequently appears as a simple isolated peak with a large intensity accounting for the important f^0 character of the initial state. The two close f_c^1 and f_c^2 configurations together with band excitations form a strongly mixed final-state continuum dominated by two leading peaks. The observation of a large intensity for states of this nature is a consequence of the existence of the $4f^1$ initial population of extended states which is in this way indirectly demonstrated. For all these $3d$ core-level spectra, the agreement between the model calculation and each spin-orbit-split component of the XPS spectra is striking and requires no further comment.

V. SYSTEMS WITH $4f^1$ GROUND-STATE CONFIGURATION IN THE UNCOUPLED SCHEME

In Figs. 3(a) and 3(b) the outer and core-level excitation spectra for CeCo$_2$, CeN, α-Ce, and γ-Ce are presented, respectively. They have been selected and displayed vertically according to increasing f occupation n_f in the ground state. The common property of these materials is

the $4f^1$ configuration of their uncoupled ground state, obtained from the best fit of the model calculation to the experimental spectra, as shown in Fig. 3(a). For these materials the total energy is larger in both the $4f^0$ (electron-subtraction) and in the $4f^2$ (electron-addition) configuration). The uncoupled f^0 and f^1 total-energy positions are not far from degeneracy allowing for a mixing of these two configurations when the coupling strength Δ becomes sizable. For these conditions the model calculation yields the peculiar excitation spectra displayed in the second column of Fig. 3(a). The BIS excitations show essentially two peaks corresponding roughly to the energy positions of the f^1 and f^2 configurations in the uncoupled $S(E_t)$. On the other hand, the XPS excitations are a mixture of f^0 and f^1 configurations producing a continuum of states with a characteristic two-peak intensity distribution. This spread of f intensity over the whole bandwidth is particularly evident for CeCo$_2$ and α-Ce where it reflects the more covalent character of the f charge. We note that this interpretation is fully consistent with the results from ground-state band calculations.[51]

With decreasing coupling strength Δ or/and increasing total-energy separation between f^0 and f^1 configurations, the outer-level excitation spectra tend to become similar to the ones known for the localized f states in heavy rare-earth materials. in γ-Ce most of the spectral weight is

found at the uncoupled f^0 and f^2 energy positions and the ground-state f occupation n_f approaches unity. It is also evident from the calculated spectra that the increase of n_f is correlated with a decrease in total energy for the $4f^2$ excitation.

For a comparison between theory and experiment only the area of the corresponding $4f$ signals must be considered, since multiplet splitting has not been included in the many-body calculation. For $CeCo_2$ (Ref. 52) and CeN the emission from Co d states and N p states must not be confused with f emission. Generally good agreement between calculated and measured spectra is obtained for the BIS excitations which show above the $4f^1$ peak the typical structure corresponding to the population of the $4f^2$ multiplets. Moreover, the predicted weight transfer from f^1 to f^2 final states is confirmed in the sequence $CeCo_2$ to γ-Ce. In the XPS spectra of $CeCo_2$ and CeN the small cross-section ratio between f and valence states impedes the observation of the $4f$ contribution in the region of the other band electrons. For α-Ce and γ-Ce, however, the data are taken from resonant photoemission work[36] where the enhancement of the f contribution allows an easier comparison with the model. In this case the overall agreement between experiment and calculation is satisfactory, especially the predicted decrease of the ratio between the f intensity at the Fermi level, and at ~ 2 eV is noticeable in the data.

The rather unique case of the metallic compound CeN deserves special interest.[41] The uncoupled $S(E_t)$, with a p valence band separated by a small gap from the d conduction band, exhibits a close similarity with the electronic structure of the insulator CeO_2. However, in contrast to CeO_2, only three electrons of Ce are necessary to complete the p band of N in CeN. For this reason the p-f mixing remains small, despite the rather important coupling parameter $\Delta_{fp} = 0.2$ eV and the small energy difference between f^1 and f^0. This situation is reflected in the spectra by the fact that very little f intensity is spread over the p band. On the other hand, the remaining f electron plays an important role in the formation of the metallic state in CeN. In the uncoupled scheme the f^1 total energy is about at the bottom of the d band so that the coupling $\Delta_{fd} = 0.1$ eV is responsible for the metallic state of this compound. The calculation yields a fractional f occupation $n_f = 0.8$ in the ground state. This description is dictated by the choice of parameters producing the best agreement of the many-body calculation with the $4f$ and core excitations (see below). A recent ground-state band calculation is also compatible with this description of the extended states.[53] The moderate value of Δ_{fp}, the very small f^0-f^1 energy difference and the fact that a single electron is involved in the hopping mechanism $f^0d^1 \leftrightarrow f^1d^0$ seems to provide in CeN the most favorable conditions for the mixing mechanism called valence fluctuation.

Finally, we have to mention that an *ab initio* supercell band-structure calculation for the outer-level excitations in Ce and Ce compounds[54] is in qualitative agreement with the electronic states description obtained in the present analysis of the experimental spectra. CeN is also found to have a peculiar behavior. It is interesting to note

that an f occupancy of ~ 0.8 is obtained for CeN, in quantitative agreement with the present calculation.

The creation of a core hole in these materials raises the total energy of the initial $4f^0$ state by ϵ_c. Then, according to Fig. 1(b) and Table I, the interactions U_{fc} and U_{ff} lead to the uncoupled final-state positions of the relevant $4f$ configurations displayed in Fig. 3(b). The uncoupled f_c^1 and f_c^2 final states are not too far from degeneracy, while the $4f_c^0$ state remains well separated from them. The situation in the presence of a core hole is thus markedly different from the one without a core hole, where the f^0 and f^1 configurations are nearly degenerate and the f^2 state has a considerably higher total energy [cf. Fig. 3(a)]. If now the hybridization is taken into account, the interaction with the band continua allows the mixing of the f_c^1 and f_c^2 configurations in the final state, giving rise to the calculated excitation spectra, shown in column 2 of Fig. 3(b). For an important coupling, like in $CeCo_2$ and CeN, this mixing between f_c^1 and f_c^2 final states is strong in each of the two peaks around 10 eV below ϵ_c. With decreasing hybridization, the intensity of the structure at the lowest total energy decreases, allowing in α-Ce and γ-Ce for a traditional identification of the two structures in terms of $4f_c^1$ and $4f_c^2$ final-state populations. On the other hand, as a consequence of the large energy separation, the f_c^0 final state at ϵ_c remains essentially pure even for the strong coupling occurring in CeN and $CeCo_2$ and their intensity evolution reflects rather well the f^0 populations $(1 - n_f)$ of the different ground states.[23]

At first sight, the comparison between calculated and measured XPS $3d$ core-level spectra may appear to be rather difficult since the $3d_{5/2}$-$3d_{3/2}$ spin-orbit components overlap partially in the middle of the spectra. However, the n_f-dependent intensity of the structures corresponding to the uncoupled f_c^0 final state is most clearly seen in the $3d_{3/2}$ component at high total energies, whereas the Δ-dependent changes in the two-peak structure, corresponding to the mixing of the uncoupled f_c^1 and f_c^2 final states, can be easily observed in the $3d_{5/2}$ component at low total energies. The comparison reveals a remarkable correspondence between calculated and observed spectral shape for CeN, α-Ce, and γ-Ce. For $CeCo_2$ the structures predicted by the calculation below ϵ_c seem to be washed out in the experimental spectrum. This effect is most probably due to the multiplet splitting which is not included in the model calculation or to lifetime broadening.

The outer- and core-level excitations for these materials with uncoupled $4f^1$ ground-state configurations are very well described by the GS model. Two conditions for the observation of unconventional excitation spectra are encountered: two configurations are nearly degenerate and a sizable coupling of the f states with the band states occurs. We want to point out once more that the two configurations f^1 and f^2 which have well-separated total energies do not mix at moderate hybridization in the outer-level excitations but they may do so in the presence of a core hole. Consequently, the intensities of the two structures resulting from their mixing in core-level spectra are by no means representative of f^1 and f^2 ground-state populations.

VI. EELS VERSUS XPS CORE-LEVEL SPECTRA

The use of the electron-energy loss spectroscopy (EELS) as a core-level spectroscopy requires a sufficiently high primary energy (1500 eV) in order to observe and analyze the electrons escaping the sample after having ionized a core level. We present in Figs. 2(b) and 3(b) the losses corresponding to the transitions from the $3d$ shell to the first unoccupied levels. In contrast to XAS processes, the EELS processes are not submitted to strict selection rules, only for primary energies much larger than the energy of the transition and at very small momentum transfer, the dipole selection rules are approximately obeyed. However, in the intermediate-energy range, it is established that the $3d \rightarrow 5d$ single-particle matrix elements are negligible when compared to those determining the intensity of the $3d \rightarrow 4f$ transitions. For this reason within the sudden approximation, the EELS many-body matrix element contains only a creation operator for an f state. This is quite different from the XPS transitions where a high-energy free electron is created. The important consequences of this difference in the core-level spectra can be easily understood schematically by considering the two types of transitions within the simplified framework of the Hamiltonian without hopping terms (see Sec. III). The mixing between two configurations is made artificially impossible so that an f^n initial state is projected only on an f_c^n final state in XPS and only on an f_c^{n+1} final state in EELS. The introduction of the coupling terms does not change very much from this situation for EELS processes where the initial configuration has a nearly integral population f^n: in the final state, the excited electron is forced to occupy an f orbital so that usually the best screened state f_c^{n+1} is naturally formed. On the other hand, for fractional f occupations, final-state mixing will necessarily take place in EELS. The situation is quite different for XPS processes where the frozen initial configuration has no longer the lowest available total energy in the presence of a core hole (except for Ba and LaF_3). In this case, different final states must be realized in order to produce the correct mean energy required by the sudden approximation.

The EELS spectra referenced to the primary energy of the beam provide a straightforward measure of the energy involved in the transitions. For technical reasons it is not possible to obtain absolute transition energies directly from XPS core-level spectra. However, with the assumption proposed in Sec. III concerning the location of the screening charge among the outer states, a common total-energy scale for XPS and EELS is simply obtained by a calibration. In fact, the same assumptions are used in the model calculation in order to represent on a common energy scale the computed XPS (solid line) and EELS (dotted line) spectra [Figs. 2(b) and 3(b)]. The multiplet splitting, particularly important in EELS,[55,56,37] has not been incorporated into the calculation. In order to make the comparison easier, the centers of gravity of the EELS final states have been calculated and their positions are indicated by arrows in the corresponding XPS and EELS spectra.

The agreement between calculated and measured rela-

tive energy positions in XPS and EELS is striking. Therefore we refrain from a detailed discussion of the spectra and comment only on a few points of specific interest. It is particularly satisfying to observe that the calculated crossing of f_c^1 and f_c^0 uncoupled positions in the sequence Ba, La_2O_3, La is fully confirmed by the experiment. The fact that the EELS final-state position in La_2O_3 is near the center of gravity of the XPS excitations proves directly the different character of the corresponding final states. It verifies experimentally the validity of the sudden approximation requiring for this particular case of a nearly pure f^0 initial state that the mean final-state energies observed in XPS and EELS spectra correspond approximately to the positions of the uncoupled configurations f_c^0 and f_c^1, respectively.

A weak satellite present in the calculated spectra for fractional occupation in EELS is also clearly visible in CeO_2 and (less prominent) in $CeCo_2$. In addition, the observed EELS structures for these systems differ from the characteristic multiplets corresponding to nearly integral f^1 or f^2 final-state populations.[56,37,57] These facts reflect the consequences of the initial-state mixing in the final state. However, in order to analyze this mixing in detail for the experimental EELS spectra, a many-body theory including multiplet splitting is needed.

VII. $L_{II,III}$ ABSORPTION EDGES VERSUS XPS CORE LEVELS

The $2p \rightarrow 5d$ photoabsorption processes involved in $L_{II,III}$ absorption edges can be considered as identical in first approximation to those occurring in the XPS ionization of any deep core level. The dipole selection rules offer to the excited electron only the possibility to occupy an extended ϵd band state. The basic Hamiltonian does not include Coulomb correlation energies between band electrons and the localized electrons, the core and f electrons. No hybridization between core and band electrons is included and coupling between f and ϵd electrons is forbidden by symmetry. The quantity $W^2(\epsilon)$ includes the dipole matrix element for absorption and the single-particle density of states. For the present calculations we have ignored the details of the energy dependence of W^2 and assumed a smooth form: $W^2(\epsilon) = \sqrt{\epsilon} e^{-\epsilon/\lambda}$, where λ is an adjustable parameter. As our Hamiltonian does not provide a coupling between the outgoing ϵd electron and the remaining electronic system, the excitation process is the same as the one for XPS core spectroscopy. The analogy with a XPS process becomes obvious: for one particular transition the sudden approximation matrix element is identical to the one for the XPS transition which involves the energy $\hbar\omega - \epsilon$ and has the spectral weight $\rho_c^{XPS}(\hbar\omega - \epsilon)$. This last quantity is precisely the intensity of the $3d$ core-level spectra computed with the model calculation and shown in Figs. 2(b) and 3(b). Within this simple Hamiltonian, the total absorption at the photon energy $\hbar\omega$ is given by the following convolution:

$$\rho_{p \rightarrow d}^{XAS}(\hbar\omega) = \int d\epsilon \, W^2(\epsilon) \rho_c^{XPS}(\hbar\omega - \epsilon) .$$

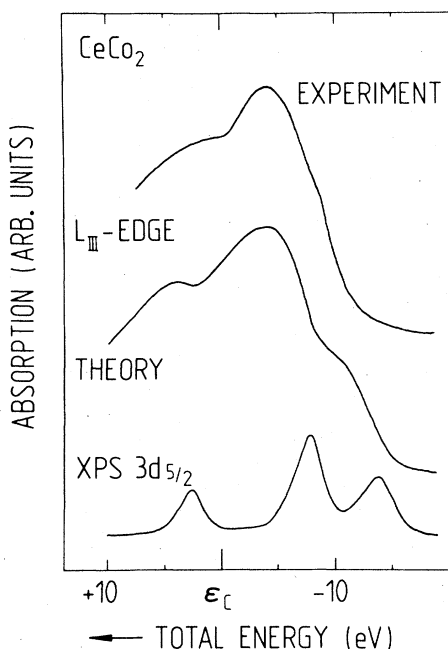In order to define the XAS spectra on the common energy scale of the other core-level spectroscopies, it has to be

FIG. 4. Calculated and measured L_{III} absorption edge for CeCo$_2$. The calculated edge is obtained by convolution of the XPS $3d_{5/2}$ core spectrum with the function $W^2(\epsilon)=\sqrt{\epsilon}\,e^{-\epsilon/\lambda}$ (see Sec. VII). The experimental spectrum was taken from Ref. 58.

represented as a function of $\hbar\omega-\epsilon_c$. This expression obtained for the $L_{\text{II,III}}$ edges is nothing else than a XPS core-level spectrum washed out by the convolution with the function $W^2(\epsilon)$.

Figure 4 shows a comparison between the measured[58] and calculated L_{III} edge of CeCo$_2$. The model calculation of the $3d$ XPS core-level spectrum presented in Fig. 3(b) and the function $W^2(\epsilon)$ with $\lambda=7$ eV have been used for this computation. The three distinct peaks in the XPS spectrum can be recognized as attenuated and broadened structures in the L-edge spectrum. In view of the approximations made in the model, the overall agreement in position and intensities between the calculated and measured spectral features is surprisingly good. Similar comparisons attempted for La$_2$O$_3$, CeO$_2$, α-Ce, and γ-Ce are less satisfactory but they still confirm that this model is a correct first approximation. Obviously the real form of $W^2(\epsilon)$ and other possible interactions of the excited electrons with the outer electrons of the solid need to be taken into account.

Quite often in such systems, the $L_{\text{II,III}}$ edges have been analyzed as if they were formed of overlapping Lorentzian lines and their intensity ratios were considered to reflect directly the configuration mixing in the initial state. This analysis has been promoted as an accurate standard technique for determining the valence.[59-65] Within the formalism proposed in the present paper, it is not possible to find any sound foundation for such an analysis and to attribute any physical meaning to the valence determined in this way.

VIII. CONCLUSION

The light rare-earth solids offer a unique possibility to investigate the different spectroscopic manifestations resulting from the coupling of an atomiclike $4f$ state with extended band states. In order to avoid complicated multiplet effects, the present study has been limited to the elements Ba, La, and Ce which contain at most one occupied $4f$ state. The orbit of these $4f$ states has just the critical dimension to give rise to a sizable mixing with wave functions of neighbor atoms but the resulting hybridized states can hardly be classified either as localized or extended. For this reason, the excitation spectra of these systems show many unconventional aspects which can be explained neither within the atomiclike model nor within the bandlike model which are commonly used in clear-cut situations. At the present time, the Anderson impurity model appears to provide the simplest framework containing the essential aspects of this problem. The success of this model applied to the calculation of the different spectroscopic excitations (Gunnarsson-Schönhammer model) settles its validity for describing the $4f$ and core-level spectra when they are observed with the usual resolution (0.1–0.5 eV) currently achieved in experiments. The apparently hidden aspects of the full many-body calculations can be easily deciphered when the meaning and the interplay of the different parameters defined in the Anderson Hamiltonian are discussed in a conventional description. Without coupling terms, this Hamiltonian provides a schematic location of the initial and final states on a total-energy scale. This approach offers an easy way to recognize the critical situations where the energy degeneracy of configurations with different f counts, together with a non-negligible wave function overlap of f states with band states (sizable Δ), give rise to a strong hybridization. Surprisingly, it took a very long time to realize that this conventional concept of hybridization, already invoked in the early photoemission studies of satellites, provides the simplest suitable framework for interpreting high-energy excitations in rare-earth solids. The challenge is now to refine the many-body theory and to improve the experimental resolution in order to elucidate the mechanisms giving rise to the valence fluctuation and heavy-fermion manifestations.

APPENDIX

Some details of a lowest-order theory are presented here. A rectangular band is assumed and f^1 admixture in the ground state is neglected. This approximation to the higher-order theory used for the calculation of the excitation spectra shown in Figs. 2 and 3, is sufficient to account qualitatively for the features in the spectra of the

Ba- and La-based materials.

The photocurrent is proportional to the spectral density:

$$\rho(e) = \frac{1}{\pi} \mathrm{Im} \langle \phi_0 \mid \psi_c^\dagger [e - i\delta - E_0 + H(N-1)\psi_c] \phi_0 \rangle$$

$$= \frac{1}{\pi} \mathrm{Im} g(e - i\delta) .$$

E_0 denotes the ground-state energy neglecting f^1 admixture. The Green's function has the form[23]

$$g(z) = \frac{1}{z - N_f \widetilde{\Gamma}(z)} ,$$

with

$$\widetilde{\Gamma}(z) = \int_{-B}^{0} \frac{V^2(\epsilon) d\epsilon}{z + \epsilon_f - U_{fc} - \epsilon} .$$

V is the hybridization matrix element defined by the hybridization parameter $\Delta = \pi \max[V^2(\epsilon)]$, ϵ_f is the energy of the f level and U_{fc} is the f electron—core-hole attraction. The core spectrum shows two characteristic features which become a prominent two-peak structure for the insulating La compounds. These two structures are due to the two poles at $\epsilon = N_F \widetilde{\Gamma}(\epsilon)$ of g always present for a rectangular band (of finite width) or for sufficiently strong hybridization. The pole strength is equal to the weight of the f^0 configuration in the final state:

$$\left[1 - N_f \frac{\partial}{\partial z} \widetilde{\Gamma}(z) \Big|_{z = N_f \widetilde{\Gamma}(z)} \right]^{-1} = W(f^0) ,$$

where the ground state is further simplified to $\phi_0 \mid 0 \rangle$. In the case where one of the poles has considerably more weight than the other, it is justifiable to label the larger peak f^0 and the other f^1. We note that in such a case the separation in the $\Delta \to 0$ limit (where the f^1 peak intensity vanishes), is of the order of $\epsilon_f - U_{fc} \sim 3$ eV in a metal. In the case of some insulating La compounds such as La_2O_3 where the two peaks are of similar strength, it does not make much sense to label the peaks f^0 and f^1. The labels would have to be interchanged for a small variation of the system parameters. In this case where $\epsilon_f - U_{fc} \sim 0$ eV, the two peaks are both of strongly mixed character. Their separation gives a rather direct measure of the hybridization strength Δ. The minimal energy separation of the two poles Δ_{pp} is given for a rectangular band by

$$\Delta_{pp} = 2N_f \frac{\Delta}{\pi} \ln \left[\frac{\Delta_{pp} + B}{\Delta_{pp} - B} \right] .$$

In the zero-bandwidth limit $B \to 0$ with $B\Delta = \text{const}$, comparison can be made with the ligand-field cluster model.[29] In this limit the minimal peak separation is $\Delta_{pp}^2 = 4N_f \Delta B / \pi$; further simplification in the ligand field model with one ligand orbital yields $\Delta_{pp} = 2V_{LF}$. On this basis our $N_f \Delta$ of ~ 5 eV is comparable to $V_{LF} \sim 2.4$ eV. For finite bandwidth B the impurity model has a continuum contribution to the core XPS spectrum at energies between the two peaks. For a rectangular band the continuum part is

$$\rho(e)_{\delta \to 0} = \frac{N_f \Delta}{[e - N_f \Delta \ln(\mid e + \epsilon_f - U_{fc} + B \mid / \mid e + \epsilon_f - U_{fc} \mid)]^2 + \pi^2 (N_f \Delta)^2} \quad \text{for} \quad U_{fc} - \epsilon_f - B < e < U_{fc} - \epsilon_f .$$

An indication for this contribution can be recognized in the experimental XPS core spectra of La_2O_3 shown in Fig. 2(b), where the "excessive intensity" between the two peaks gives rise to the characteristic tails of the two structures.

[1] T. A. Carlson, M. O. Krause, and W. E. Moddeman, J. Phys. (Paris) Colloq. 32, C4-76 (1971), and references therein.

[2] G. K. Wertheim and A. Rosencwaig, Phys. Rev. Lett. 26, 1179 (1971).

[3] A. Rosencwaig, G. K. Wertheim, and H. J. Guggenheim, Phys. Rev. Lett. 27, 479 (1971).

[4] C. K. Jørgensen and H. Berthou, Chem. Phys. Lett. 13, 186 (1972).

[5] G. K. Wertheim, R. L. Cohen, A. Rosencwaig, and H. J. Guggenheim, in Electron Spectroscopy, edited by D. A. Shirley (North-Holland, 1972), p. 813.

[6] A. Signorelli and R. G. Hayes, Phys. Rev. B 8, 81 (1973).

[7] S. Suzuki, T. Ishii, and T. Sagawa, J. Phys. Soc. Jpn. 37, 1334 (1974).

[8] S. Hüfner, in Photoemission in Solids II, Vol. 27 of Topics in Applied Physics, edited by L. Ley and M. Cardona (Springer, New York, 1978), p. 173.

[9] C. K. Jørgensen, Struct. Bonding (Berlin) 13, 199 (1973); 24, 1 (1975).

[10] B. W. Veal and A. Paulikas, Phys. Rev. Lett. 51, 1995 (1983); Phys. Rev. B 31, 5399 (1985).

[11] D. F. Mullica, C. K. C. Lok, H. O. Perkins, and V. Young, Phys. Rev. B 31, 4039 (1985).

[12] Y. Baer, in Handbook on the Physics and Chemistry of the Actinides, edited by A. J. Freeman and G. Lander (North-Holland, Amsterdam, 1984), p. 271.

[13] W. D. Schneider and C. Laubschat, Phys. Rev. Lett. 46, 1023 (1981).

[14] J. F. Herbst and J. W. Wilkins, Phys. Rev. Lett. 43, 1760 (1979).

[15] A. Kotani and J. Toyozawa, J. Phys. Soc. Jpn. 35, 1073 (1973); 35, 1082 (1973); 37, 912 (1974).

[16] A. Kotani, Jpn. J. Phys. 46, 488 (1979).

[17] K. Schönhammer and O. Gunnarsson, Solid State Commun. 23, 691 (1977); 26, 147 (1978); 26, 399 (1978); Z. Phys. B 30, 297 (1978).

[18] R. Manne and T. Åberg, Chem. Phys. Lett. 7, 282 (1970).

[19] P. Burroughs, A. Hamnett, A. F. Orchard, and G. Thornton,

J. Chem. Soc. Dalton Trans. **17**, 1686 (1976).

[20]G. Crecelius, G. K. Wertheim, and D. N. E. Buchanan, Phys. Rev. B **18**, 6519 (1978).

[21]J. C. Fuggle, M. Campagna, Z. Zolnierek, R. Lässer, and A. Platau, Phys. Rev. Lett. **45**, 1597 (1980).

[22]S. J. Oh and S. Doniach, Phys. Rev. B **26**, 2085 (1982).

[23]O. Gunnarsson and K. Schönhammer, Phys. Rev. Lett. **50**, 604 (1983); Phys. Rev. B **28**, 4315 (1983).

[24]J. C. Fuggle, F. U. Hillebrecht, J.-M. Esteva, R. C. Karnatak, O. Gunnarsson, and K. Schönhammer, Phys. Rev. B **27**, 4637 (1983).

[25]J. C. Fuggle, F. U. Hillebrecht, Z. Zolnierek, R. Lässer, Ch. Freiburg, O. Gunnarsson, and K. Schönhammer, Phys. Rev. B **27**, 7330 (1983).

[26]F. U. Hillebrecht, J. C. Fuggle, G. A. Sawatzky, M. Campagna, O. Gunnarsson, and K. Schönhammer, Phys. Rev. B **30**, 1777 (1984).

[27]E. Wuilloud, H. R. Moser, W.-D. Schneider, and Y. Baer, Phys. Rev. B **28**, 7354 (1983).

[28]E. Wuilloud, W.-D. Schneider, B. Delley, Y. Baer, and F. Hulliger, J. Phys. C **17**, 4799 (1984).

[29]A. Fujimori, Phys. Rev. B **28**, 2281 (1983).

[30]S. Hüfner and P. Steiner (unpublished).

[31]G. K. Wertheim, in *Valence Fluctuations in Solids*, edited by L. M. Falicov, W. Hanke, and M. B. Maple (North-Holland, Amsterdam, 1981), p. 67.

[32]F. Riehle, Jpn. Journal of Appl. Phys. **17**, Suppl. 17-2, 314 (1978).

[33]J. Kanski and G. Wendin, Phys. Rev. B **24**, 4977 (1981).

[34]S. Sato, J. Phys. Soc. Jpn. **41**, 913 (1976).

[35]P. Motais, E. Belin, and C. Bonelle, Phys. Rev. B **30**, 4399 (1984).

[36]N. Mårtensson, B. Reihl, and R. D. Parks, Solid State Commun. **41**, 573 (1982).

[37]H. R. Moser, B. Delley, W.-D. Schneider, and Y. Baer, Phys. Rev. B **29**, 2947 (1984).

[38]J. K. Lang, Y. Baer, and P. A. Cox, J. Phys. F **11**, 121 (1981).

[39]E. Wuilloud, B. Delley, W.-D. Schneider, and Y. Baer, Phys. Rev. Lett. **53**, 202 (1984); **53**, 2519 (1984).

[40]Y. Baer and Ch. Zürcher, Phys. Rev. Lett. **39**, 956 (1977).

[41]E. Wuilloud, B. Delley, W.-D. Schneider, and Y. Baer, J. Magn. Magn. Mater. **47-48**, 197 (1985).

[42]J. K. Lang and Y. Baer, Rev. Sci. Instrum. **50**, 221 (1979).

[43]B. Delley and H. Beck, J. Magn. Magn. Mater. **47—48**, 269

(1985).

[44]B. Delley and H. Beck, J. Phys. C **17**, 4971 (1984).

[45]D. D. Koelling, A. M. Boring, and J. H. Wood, Solid State Commun. **47**, 227 (1983).

[46]K. R. Bauchspies, W. Boksch, E. Holland-Moritz, H. Launois, R. Pott, and D. Wohlleben, in *Valence Fluctuations in Solids*, Ref. 31, p. 147.

[47]P. Wachter, in *Valence Instabilities*, edited by P. Wachter and H. Boppart (North-Holland, Amsterdam, 1982), p. 145.

[48]C. M. Varma, Rev. Mod. Phys. **48**, 219 (1976).

[49]L. Ley, N. Mårtensson, and J. Azoulay, Phys. Rev. Lett. **45**, 1516 (1980).

[50]W. Gordy and W. J. O. Thomas, J. Chem. Phys. **24**, 439 (1955).

[51]D. D. Koelling, Physica (Utrecht) **130B**, 135 (1985).

[52]Similar data can be found in Refs. 25 and 26.

[53]M. S. S. Brooks, J. Magn. Magn. Mater. **47-48**, 260 (1985).

[54]M. R. Norman, D. D. Koelling, A. J. Freeman, H. J. F. Jansen, B. I. Min, T. Oguchi, and Ling Ye, Phys. Rev. Lett. **53**, 1673 (1984); M. R. Norman, D. D. Koelling, and A. J. Freeman, Phys. Rev. B **31**, 6251 (1985).

[55]F. P. Netzer, G. Strasser, and J. A. D. Matthew, Phys. Rev. Lett. **51**, 211 (1983).

[56]J. A. D. Matthew, G. Strasser, and F. P. Netzer, Phys. Rev. B **27**, 5839 (1983).

[57]G. Kaindl, G. Kalkowski, W. D. Brewer, E. V. Sampathkumaran, F. Holzberg, A. Schach, and V. Wittenau, J. Magn. Magn. Mater. **47-48**, 181 (1985).

[58]C. N. R. Rao, D. D. Sarma, P. R. Sarode, R. Vijayaharaghavan, S. K. Dhar, and S. K. Malik, J. Phys. C **14**, 451 (1981).

[59]R. D. Parks, S. Raen, M. L. den Boer, V. Murgai, and T. Mihalisin, Phys. Rev. B **28**, 3556 (1983).

[60]S. Raen, M. L. den Boer, V. Murgai, and R. D. Parks, Phys. Rev. B **27**, 5139 (1983).

[61]E. Beaurepaire, G. Krill, J. P. Kappler, and J. Röhler, Solid State Commun. **49**, 65 (1984).

[62]D. Wohlleben and J. Röhler, J. Appl. Phys. **55**, 1904 (1984).

[63]E. V. Sampathkumaran, K. H. Frank, G. Kalkowski, G. Kaindl, M. Domke, and G. Wortmann, Phys. Rev. B **29**, 5702 (1984).

[64]J. Röhler, J. Magn. Magn. Mater. **47-48**, 175 (1985).

[65]H. Jhans and M. Croft, J. Magn. Magn. Mater. **47-48**, 203 (1985).